Macromolecules

ARTICLE

pubs.acs.org/Macromolecules

Nanoparticle-Based and Organic-Phase-Based AGET ATRP PolyHIPE Synthesis within Pickering HIPEs and Surfactant-Stabilized HIPEs

Inna Gurevitch and Michael S. Silverstein*

Department of Materials Engineering, Technion - Israel Institute of Technology, Haifa 32000, Israel

ABSTRACT: PolyHIPEs are porous polymers synthesized within high internal phase emulsions (HIPEs). Recent research has shown that the locus of conventional free radical initiation (at the oil−water interface or in the organic phase) can affect the polyHIPE's structure and properties. This paper is the first investigation of polyHIPE synthesis using activators generated by electron transfer for atom-transfer radical polymerization (AGET ATRP). Two different types of initiators (organic-phase-based and nanoparticle-based) were used to synthesize polyHIPEs within both surfactant-stabilized HIPEs and nanoparticle-stabilized Pickering HIPEs. The type and locus of initiation affected the macromolecular structure for all the polyHIPEs. Furthermore, the initiator also affected both the porous structure and the wall structure of polyHIPEs synthesized within Pickering HIPEs. Depending upon the initiator, either a polyhedral void shape or a nanoparticle assembly at the interface could become "locked in" at the very beginning of the polymerization.

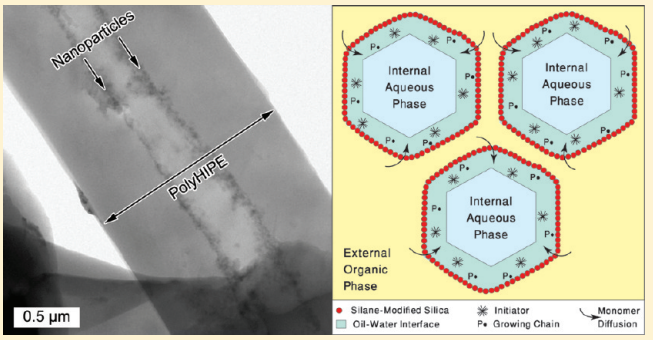

INTRODUCTION

PolyHIPEs, polymers synthesized through the polymerization of monomers in the external phase of high internal phase emulsions (HIPEs), emulsions with over 74% internal phase, have been described in some detail.[1−8] A variety of polyHIPEs and polyHIPE-based materials have been synthesized, including copolymers,[9,10] interpenetrating polymer networks,[11] crystallizable side-chain polymers,[12−14] hydrophilic polymers,[15−19] biocompatible polymers,[20−25] functional surfaces,[26,27] organic−inorganic hybrids,[28,29] composites,[30−37] and ultralow-density polymers.[38] PolyHIPEs are usually synthesized through chain-growth polymerization using conventional free radical initiators, although step-growth and ring-opening polymerizations have also been investigated[39,40] Water-soluble or organic-soluble initiators can be used to synthesize polyHIPEs, and the initiator can be added to either the internal phase or the external phase. PolyHIPEs have also been synthesized using initiators in both phases and/or using monomers in both phases.[41,42] Most commonly, HIPEs have a hydrophobic external phase containing monomers and an aqueous internal phase containing a water-soluble initiator. Thus, initiation usually takes place at the oil−water interface. The locus of initiation, whether interfacial initiation or organic-phase initiation, has been shown to have significant effects upon the structure and properties of polyHIPEs.[14,41,43]

HIPEs are usually stabilized through the use of a relatively large amount of organic surfactant (20−30% of the external phase). Surfactant-free Pickering emulsions are stabilized by particles that migrate to the oil−water interface.[44−46] Recent work has demonstrated that polyHIPEs can also be synthesized within Pickering HIPEs.[47−51] The locus of initiation can also have a significant effect upon the void structure in polyHIPEs from Pickering HIPEs.[43] Interfacial initiation can "lock in" the polyhedral structure of the HIPE's internal phase since the polymerization begins at the interface. Organic-phase initiation can produce larger, spherical voids that reflect HIPE destabilization during polymerization.

The synthesis of polyHIPEs using atom-transfer radical polymerization (ATRP) has not been investigated, although a brominated monomer was incorporated into polyHIPEs for a subsequent grafting step.[52] Based upon the results for conventional radical polymerization, the type and locus of initiation used for ATRP could also have a significant effect upon the polyHIPE structure and properties. HIPEs usually contain both an organic phase and an aqueous phase. Activators generated by electron transfer for atom-transfer radical polymerization (AGET ATRP), which has exhibited enhanced catalyst stability, would seem to be suitable for polymerizations within HIPEs.[53−59] The AGET ATRP system consists of an initiator, a transition metal catalyst, a ligand, and a reducing agent. Two types of initiator can be used for AGET ATRP. The first is an organic-soluble initiator that can be added to the external phase. The second is an initiator attached to a nanoparticle (NP) surface since ATRP initiators can be attached to solid surfaces.[52,60−64] NP-based AGET ATRP is illustrated schematically in Figure 1 wherein an alkoxysilane bearing a chloromethylphenyl initiator group is attached to the surface of a silica nanoparticle (after Matyjaszewski).[53]

Received: February 16, 2011
Revised: April 3, 2011
Published: April 15, 2011

ACS Publications © 2011 American Chemical Society

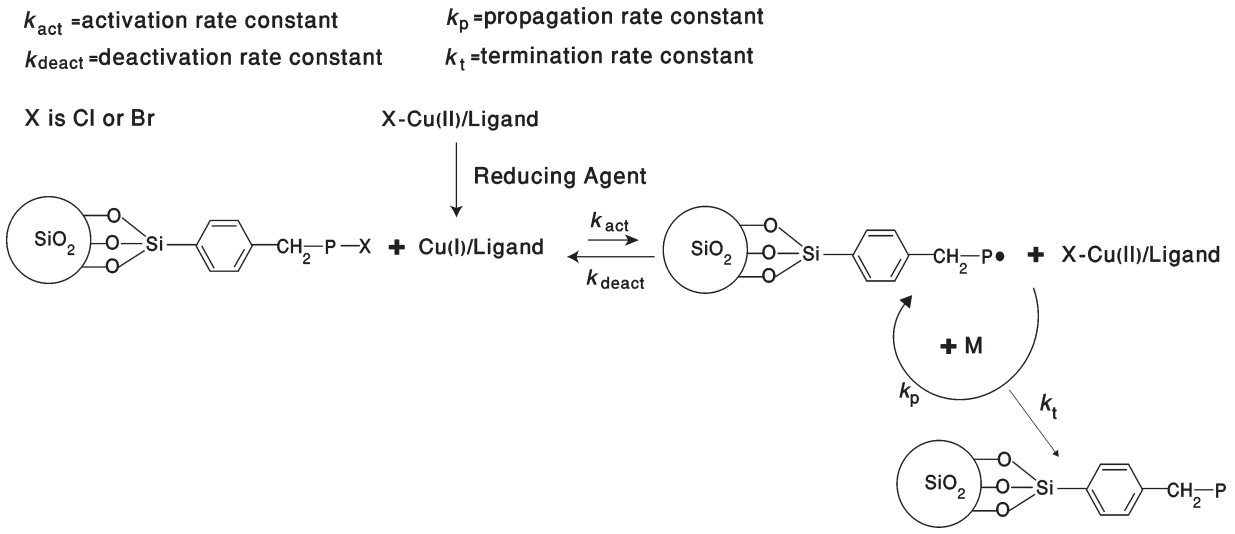

Figure 1. An NP-based AGET ATRP polymerization mechanism (after Matyjaszewski).[53]

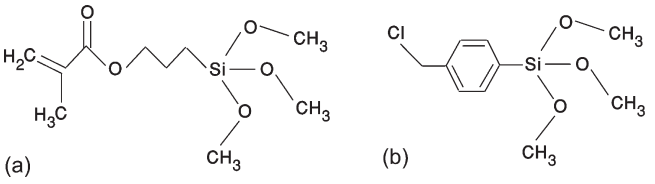

Figure 2. Scheme of (a) MPtMS and (b) CMPtMS.

This paper will describe the effects of AGET ATRP using two types of initiation (organic-phase-based and NP-based) on the polyHIPE structure and properties for both surfactant-stabilized HIPEs and Pickering HIPEs. The results from AGET ATRP initiation will be compared to those from conventional radical polymerization (interfacial initiation and organic-phase initiation).

EXPERIMENTAL SECTION

Materials. The monomer, 2-ethylhexyl acrylate (EHA, Aldrich), and cross-linking comonomer, divinylbenzene (DVB, containing 20% ethylstyrene, Aldrich), were washed to remove the inhibitor (three times with a 5 wt % sodium hydroxide solution and then three times with deionized water). The fumed silica nanoparticles had an average diameter of 7 nm and a surface area of 390 m^2/g (Sigma). In some cases the nanoparticle surface was modified using 3-methacryloxypropyltrimethoxysilane (MPtMS, 248.3 g/mol, Alfa Aesar, Figure 2a) in a solution of ethanol (Bio Lab), acetic acid (Merck), and deionized water. The surfactant used in the surfactant-stabilized HIPEs was sorbitan monooleate (SMO, Span 80, Fluka Chemie).

For reactions using AGET ATRP, a combination of $CuBr_2$ (Aldrich) and 2,2-bipyridine (bpy, Sigma) was the catalyst system, ascorbic acid (AA, Sigma) was the reducing agent, ethyl α-bromoisobutyrate (EBiB, Aldrich) was the organic-soluble initiator, and *p*-chloromethylphenyltrimethoxysilane (CMPtMS, 246.8 g/mol, Gelest, Figure 2b) was the nanoparticle-based initiator. For reactions using conventional radical polymerization, potassium persulfate ($K_2S_2O_8$, KPS, Riedel-de-Haen) was the water-soluble initiator and benzoyl peroxide (BPO, Fluka Chemie) was the organic-soluble initiator. Potassium sulfate (K_2SO_4, Frutarom, Israel) was added to the aqueous phase as a stabilization enhancer when conventional radical initiators were used, but not added for AGET ATRP.

Table 1. **HIPE Recipes (wt %)**

samples[a]		SE	SC	PKM	PBM	PEM	PC
external, organic phase	EHA	11.37	11.31	11.83	11.83	11.75	11.78
	DVB	2.93	2.92	3.05	3.05	3.03	3.04
	SMO	4.02	4.00	0	0	0	0
	M-NP	0	0	0.63	0.63	0.62	0
	C-NP	0	0.66	0	0	0	0.69
	$CuBr_2$	0.06	0.06	0	0	0.06	0.06
	bpy	0.04	0.04	0	0	0.04	0.04
	EBiB	0.20	0	0	0	0.21	0
	BPO	0	0	0	0.26	0	0
	water	1.00	1.00	0	0	1.04	1.04
	total	19.62	19.99	15.50	15.77	16.75	16.66
internal, aqueous phase	water	80.32	79.95	83.58	83.58	83.04	83.28
	AA	0.06	0.06	0	0	0.21	0.06
	KPS	0	0	0.26	0	0	0
	K_2SO_4	0	0	0.65	0.65	0	0
	total	80.38	80.01	84.50	84.23	83.25	83.34

[a] S: SMO-stabilized; P*x*M: MPtMS-modified-NP-stabilized; K: KPS-initiated; B: BPO-initiated; E: EBiB-initiated; PC: CMPtMS-modified-NP-stabilized/initiated.

Soxhlet extraction of the polyHIPE was performed using methanol (Bio Lab) and deionized water. For some polyHIPE, ultramicrotomed polyHIPE specimens for transmission electron microscopy (TEM) were prepared by infiltrating the polyHIPE with methyl methacrylate (MMA, Aldrich) containing 1 wt % BPO and polymerizing.

Silane Modification. The silane modification of the nanoparticle surface using either MPtMS or CMPtMS took place in an aqueous ethanol solution (95 vol % ethanol). The pH of the ethanol solution was adjusted to 4.5 by adding 3 vol % of an aqueous acetic acid solution (5.5 vol % acetic acid, 1 M). Either MPtMS (2.5 wt % of the solvents) or CMPtMS (5.0 wt % of the solvents) was added to the solution. The silica nanoparticles, 1.4 wt % of the solvents, were added 1 h afterward, and the mixture was stirred for 1 h. The nanoparticles were filtered using Whatman No. 1 filter paper and dried overnight in a convection oven at 70 °C. The mass ratio of MPtMS to silica was 1.8, while the mass ratio of CMPtMS to silica was 3.6, twice that of MPtMS. Given the similar

dx.doi.org/10.1021/ma200362u |*Macromolecules* 2011, 44, 3398–3409

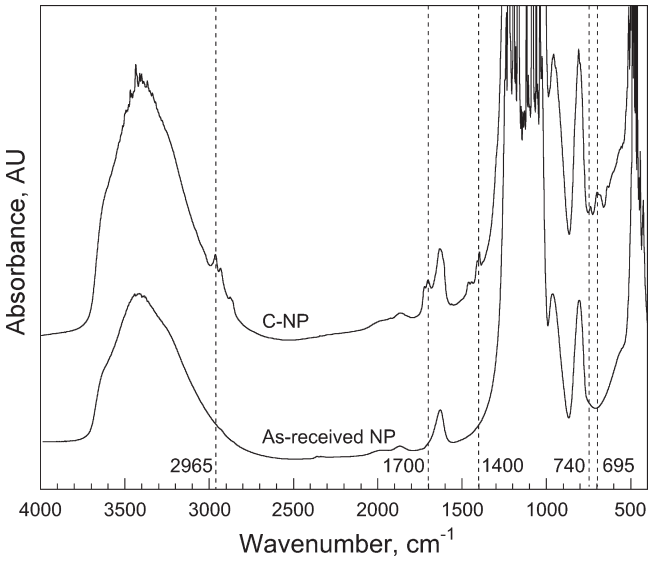

Figure 3. FTIR spectra of as-received NP and C-NP.

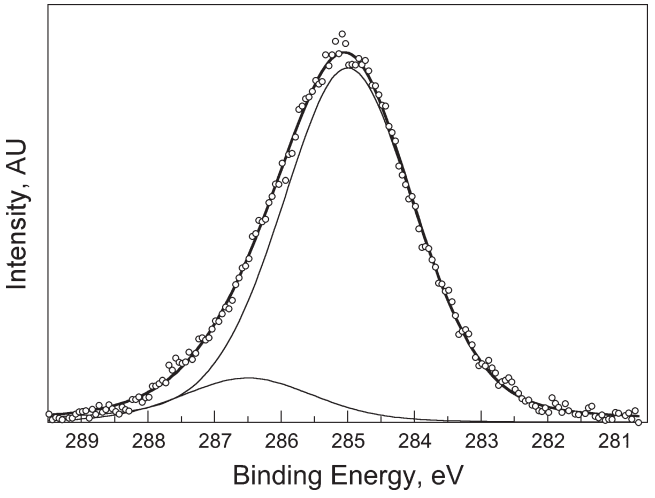

Figure 4. XPS C_{1s} spectrum from C-NP (circles), the individual peaks from curve fitting (thin lines), and the sum of the peaks (thick line).

molecular weights of CMPtMS and MPtMS, there was also twice as much CMPtMS on a molar basis. The MPtMS-modified nanoparticles are termed M-NP, and the CMPtMS-modified nanoparticles are termed C-NP.

PolyHIPE Synthesis. The different HIPE recipes are listed in Table 1. The first letter of the sample name indicates the type of HIPE stabilization (S for surfactant and P for Pickering). The second letter of the sample name indicates the type of initiator (K for KPS, B for BPO, E for EBiB, and C for C-NP). An M is added to the sample name if the sample contained M-NP. For example, two different polyHIPEs, SE and PEM, were initiated using EBiB. SE was a surfactant-stabilized HIPE, while PEM was an M-NP-stabilized Pickering HIPE. In addition, two different polyHIPEs, SC and PC, were initiated using C-NP. SC was a surfactant-stabilized HIPE, while PC was a C-NP-stabilized Pickering HIPE.

For AGET ATRP, the internal phase consisted of an aqueous AA solution. A second, identical aqueous AA solution was prepared and set aside. The catalyst system ($CuBr_2$ and bpy) was dissolved in water and then added to the organic phase. The catalyst system was added to the organic phase so that its interaction with the AA in the aqueous phase would be minimized. The organic phase was cooled in an ice bath and

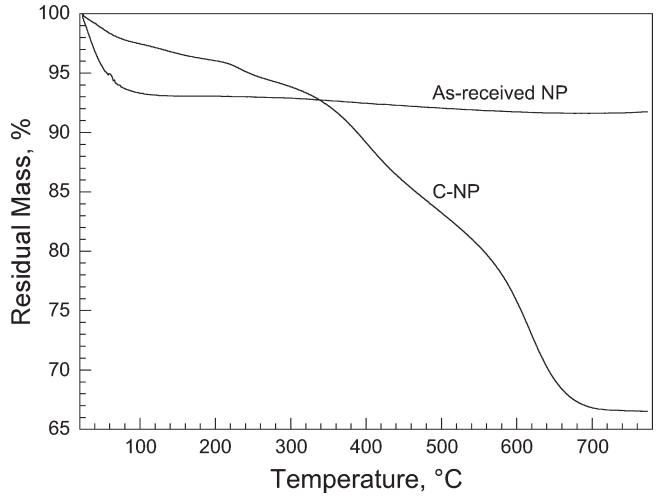

Figure 5. TGA curves from as-received NP and C-NP.

remained in the ice bath during HIPE formation. The aqueous phase was slowly added to the organic phase with continuous stirring. The AA content in the aqueous phases of SE, SC, and PC was 0.42 wt % relative to the monomer content. The AA content in the aqueous phase of PEM was 1.40 wt % relative to the monomer content. The higher AA content was used to increase the polymerization rate and thereby enhance the stability of PEM.[59] After the entire aqueous phase was added to the HIPE, the stirring was stopped and the second AA solution was poured over the HIPE. The aqueous solution above the HIPE was used to minimize the contact of the AGET ATRP components with air. The HIPEs were covered with aluminum foil and polymerized in a circulating air oven at 80 °C for 24 h (without stirring). The polyHIPEs were dried in a vacuum oven from 48 to 72 h (until a constant weight was achieved), underwent Soxhlet extraction in deionized water for 24 h, underwent Soxhlet extraction in methanol for 24 h, and were then dried in a convection oven at 80 °C for 24 h.

Two different M-NP stabilized Pickering HIPEs were synthesized using conventional free radical initiation. PKM contained a water-soluble free radical initiator added to the internal phase for interfacial initiation. PBM contained an organic-soluble free radical initiator added to the external phase for organic-phase initiation. For the conventional free radical initiated polymerizations, the synthesis procedure was similar to, but simpler than, that described above. The aqueous phase was slowly added to the organic phase with continuous stirring. The HIPEs were covered with aluminum foil and polymerized in a circulating air oven at 65 °C for 24 h (without stirring). The resulting polyHIPEs were dried in a vacuum oven from 48 to 72 h (until a constant weight was achieved), underwent Soxhlet extraction in deionized water for 24 h, and were then dried in a vacuum oven for 48 h.

Characterization. The effects of nanoparticle surface modification were characterized using Fourier transform infrared spectroscopy (FTIR, Equinox 55 FTIR, Bruker), X-ray photoelectron spectroscopy (XPS, Thermo Sigma Probe, VG Scientific), and thermogravimetric analysis (TGA, 2050 TGA, TA Instruments). The FTIR spectra from KBr pellets containing 3 wt % sample were taken from 400 to 4000 cm^{-1} at a resolution of 2 cm^{-1}. TGA was run in air from room temperature to 800 °C at 20 °C/min. The mass loss between 25 and 100 °C was associated with the evaporation of water, and the mass loss between 100 and 200 °C was associated with the pyrolysis of hydrocarbon contaminants. The mass loss between 200 and 800 °C was associated with the pyrolysis of the organic part of the silane, whose molecular weight is known. The average coverage of the silica nanoparticles by silane molecules was

estimated from the TGA mass loss between 200 and 800 °C given the known nanoparticle surface area of 390 m^2/g. The sample's surface area was estimated from the sample mass following pyrolysis. The molar content of silane originally present on the surface was estimated from the mass loss by assuming that all of the organic material was pyrolyzed. The surface coverage was calculated by dividing the moles pyrolyzed by the surface area.

The polyHIPE density, ρ, was determined using gravimetric analysis. The polymerization yield was based on the polyHIPE mass following drying. The gel content, GC, was the mass fraction that remained when the polyHIPEs were immersed for 48 h in boiling xylene and then dried in a vacuum oven. The thermal properties of the polyHIPEs were characterized using dynamic mechanical thermal analysis (DMTA) temperature sweeps at 3 °C/min in compression at a frequency of 1 Hz on 5 × 5 × 5 mm^3 cubes (DMTA IV, Rheometric Scientific).

The porous structure was characterized using low-vacuum scanning electron microscopy (SEM) of uncoated cryogenic fracture surfaces (FEI Quanta 200, 20 kV). The average polyHIPE void sizes were calculated from the SEM micrographs using a correction for the statistical nature of the cross section.[65] SE, SC, PC, and PBM were infiltrated with MMA containing 1 wt % BPO for 1 h under vacuum. The MMA was polymerized at 50 °C in a circulating air oven. Specimens

Table 2. **PolyHIPE Properties**

samples[a]	yield, %	GC, %	ρ, g/cm^3	void size, μm	tan δ peak, °C
SE	96.8	95	0.14	6−15	−20
SC	78.0	95	0.14	6−20	5
PKM	81.8	91	0.16	60−115	−27
PBM	64.1	97	0.15	310	−11
PEM	67.4	98	0.12	120−210	−27
PC	66.8	98	0.13	75−120	−11

[a] S: SMO-stabilized; P*x*M: MPtMS-modified-NP-stabilized; K: KPS-initiated; B: BPO-initiated; E: EBiB-initiated; PC: CMPtMS-modified-NP-stabilized/initiated.

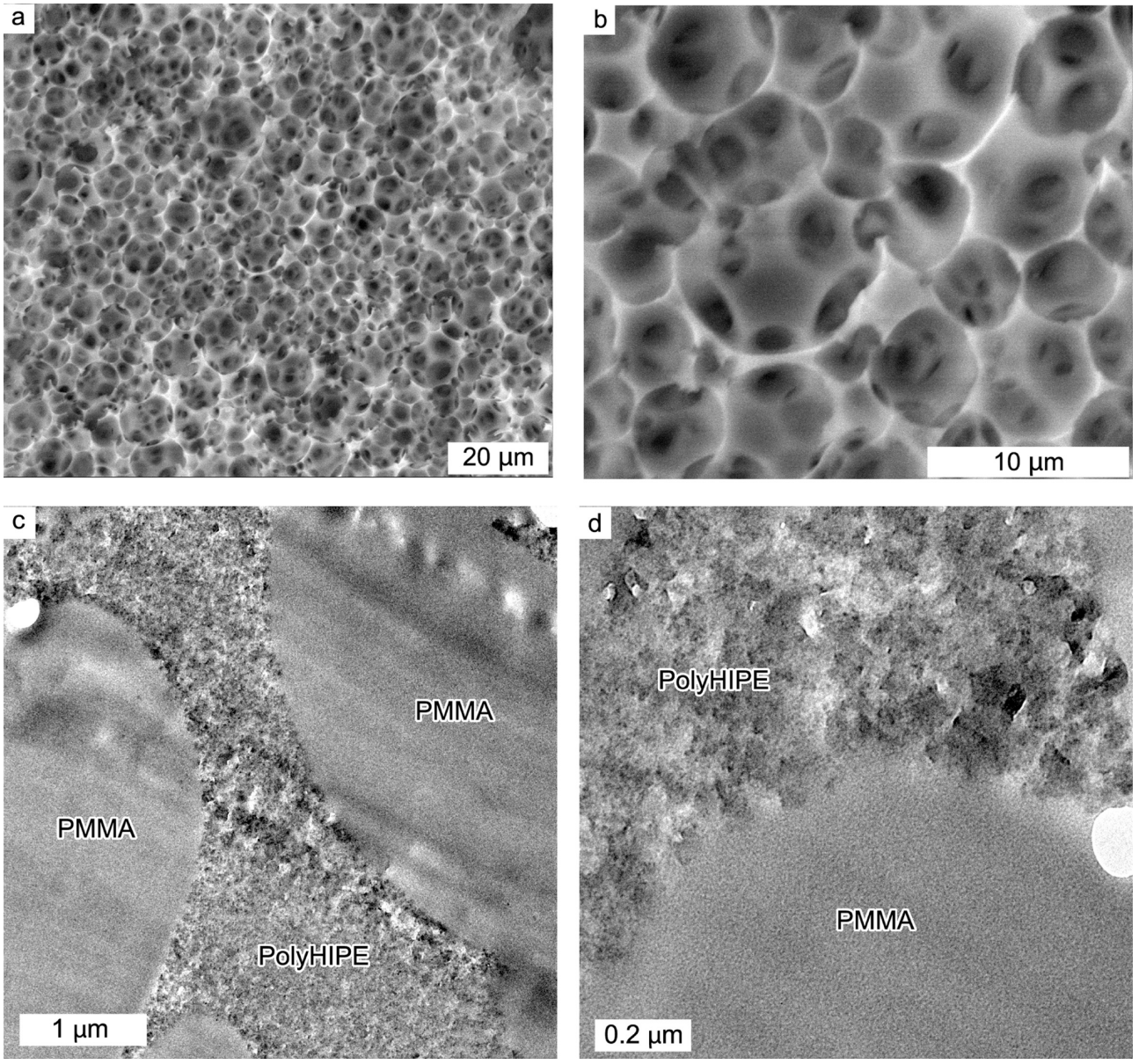

Figure 6. SE: SEM micrographs (a, b) and TEM micrographs (c, d).

dx.doi.org/10.1021/ma200362u |*Macromolecules* 2011, 44, 3398–3409

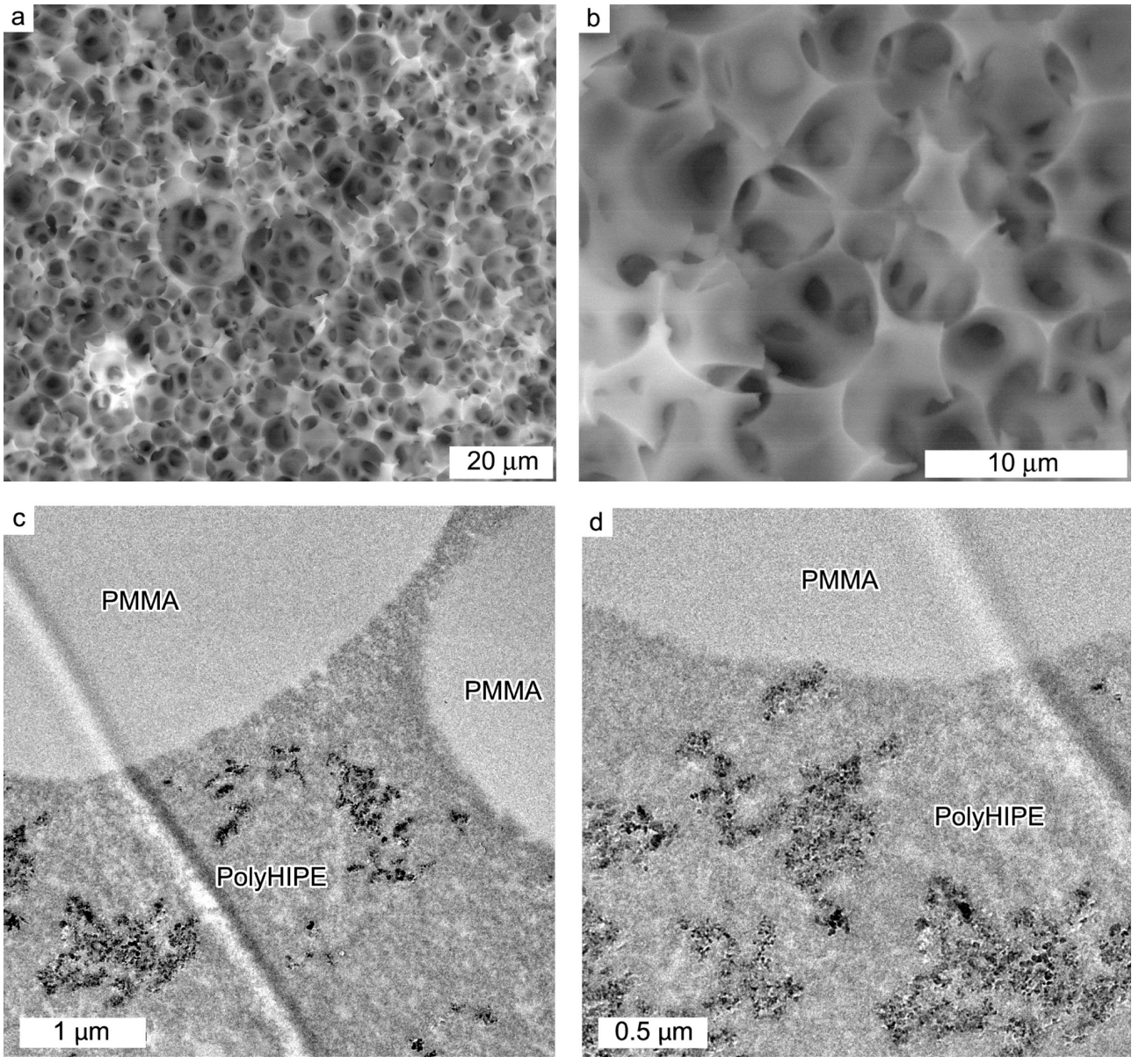

Figure 7. SC: SEM micrographs (a, b) and TEM micrographs (c, d).

70−80 nm thick were prepared from the PMMA-filled polyHIPEs using ultramicrotomy (Ultracut E, Reichert-Jung) and viewed using TEM (FEI Technai G2 T20 S-Twin, operating at 200 kV). In some cases, for PEM and PKM, the contrast between the polyHIPE and the PMMA was poor. TEM specimens were prepared from PEM and PKM prior to drying using cryo-ultramicrotomy. The water in the specimen was removed by allowing it to dry at room temperature.

RESULTS AND DISCUSSION

Surface Modification of the Nanoparticles. TGA analysis has shown that the MPtMS modification of the nanoparticle surface yields a surface coverage of 3.2 μmol/m^2.[43] The FTIR spectra from as-received NP and C-NP are presented in Figure 3. C-NP exhibits bands at 2965, 1700, 1400, and 695 cm^{-1} that are associated with the benzene ring and are not exhibited by the as-received NP. C-NP also exhibits a band at 740 cm^{-1} that is associated with CH_2Cl and was not exhibited by the as-received NP. These bands clearly demonstrate the incorporation of the chloromethylphenyl groups on the nanoparticle surface. This is confirmed by XPS analysis. The C:Cl atomic ratio in the chloromethylphenyl group is 7:1, and only one of the 7 carbons (14.3%) is bound to the chlorine atom. The C:Cl ratio from the low-resolution XPS spectrum was 5.8:1.0. These results indicate that the carbon on the C-NP surface is from the chloromethylphenyl groups and not from hydrocarbon contaminants. The high-resolution C_{1s} XPS spectrum from C-NP is presented in Figure 4. The curve fit to the C_{1s} spectrum yields two peaks using a full width at half-maximum of 2.36 eV and a Gaussian to Lorenzian ratio of 0.25. The peak at 285.0 eV, 88.8%, represents carbon−carbon bonding. The peak at 286.5 eV, 11.2%, represents carbon−chlorine bonding, the only one of the seven carbon atoms that has a carbon−chlorine bond. These results confirm that the organic material on the surface of C-NP is from the chloromethylphenyl groups.

The TGA results for the as-received NP and C-NP are presented in Figure 5. C-NP exhibits a 29.5% mass loss between 200 and 800 °C. This mass loss is attributed to the pyrolysis of the chloromethylphenyl groups. The mass loss from the as-received NP in the corresponding temperature range was negligible. A chloromethylphenyl surface coverage of 10.0 μmol/m^2 was calculated from these results, more than thrice the 3.2 μmol/m^2 found for MPtMS.[43] The higher surface coverage for CMPtMS reflects its higher concentration in the solution and, perhaps, its higher reactivity. The HIPE recipes in Table 1 were based upon this calculation. The AGET ATRP procedure described by Matyjaszewski uses an excess of initiator and the HIPE recipes were chosen such that the CMPtMS and EBiB contents would correspond.[54,55] The molar ratio of CMPtMS:$CuBr_2$:bpy:AA in SC and PC was 1.0:0.2:0.2:0.2, the same as the molar ratio of EBiB:$CuBr_2$:bpy:AA in SE. A ratio of 1.0:0.2:0.2:0.7 was used to enhance the polymerization rate in PEM, as described above.

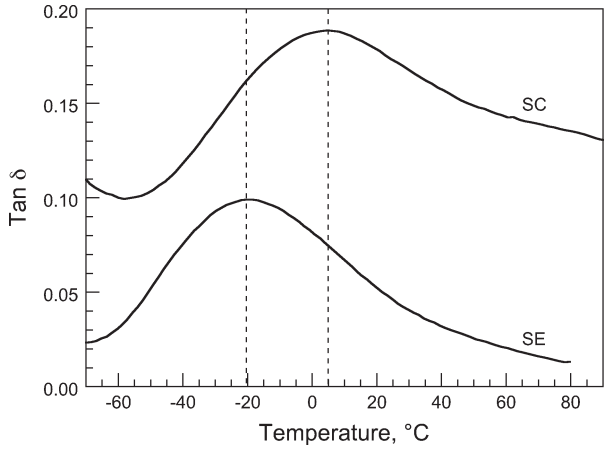

Figure 8. Tan δ curves from SE and SC.

PolyHIPE Properties. The polyHIPE properties are listed in Table 2. In general, the yields from surfactant-stabilized HIPEs are larger than those from Pickering HIPEs.[43] The yields from the AGET ATRP polyHIPEs in Table 2 (SE, PEM, SC, PC) were comparable to the yields from similar HIPE recipes that were polymerized using conventional free radical initiators (PKM, PBM). Here, too, the yields from surfactant-stabilized HIPEs (SE and SC) were somewhat larger than those from the corresponding Pickering HIPEs (PEM and PC, respectively). The relatively high yield in SE reflects the enhanced HIPE stability from SMO and the higher efficiency of EBiB. All the polyHIPEs have gel contents of over 90% and densities of around 0.14 g/cm^3. The similarities in gel content and in density reflect the similar DVB contents and the similar aqueous phase contents, respectively (Table 2).

AGET ATRP in Surfactant-Stabilized HIPEs. The structure of a polyHIPE can be described using a set of micrographs taken at different magnifications. The porous structure is portrayed using SEM micrographs, and the internal wall structure is portrayed using TEM micrographs. The porous structures of the two polyHIPEs based on surfactant-stabilized HIPEs, EBiB initiated SE (Figure 6a,b) and C-NP initiated SC (Figure 7a,b), are quite similar to each other. These porous structures are also quite similar to equivalent conventional free radical initiated polyHIPEs based upon surfactant-stabilized HIPEs.[43] The voids in SE and SC range from 6 to 20 μm in diameter, and the porous structure is highly interconnected. Figure 6a,b and Figure 7a,b

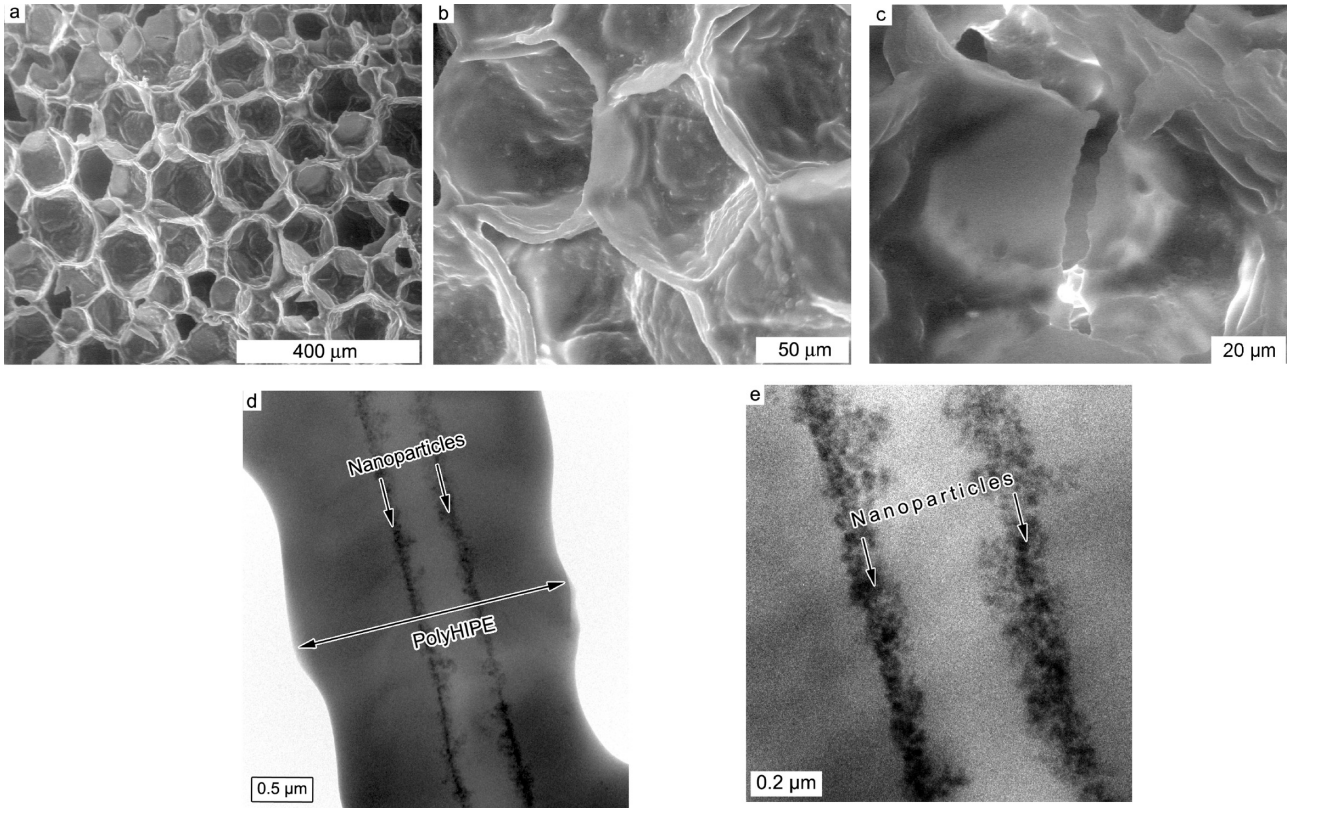

Figure 9. PKM: SEM micrographs (a−c) and TEM micrographs (d, e).

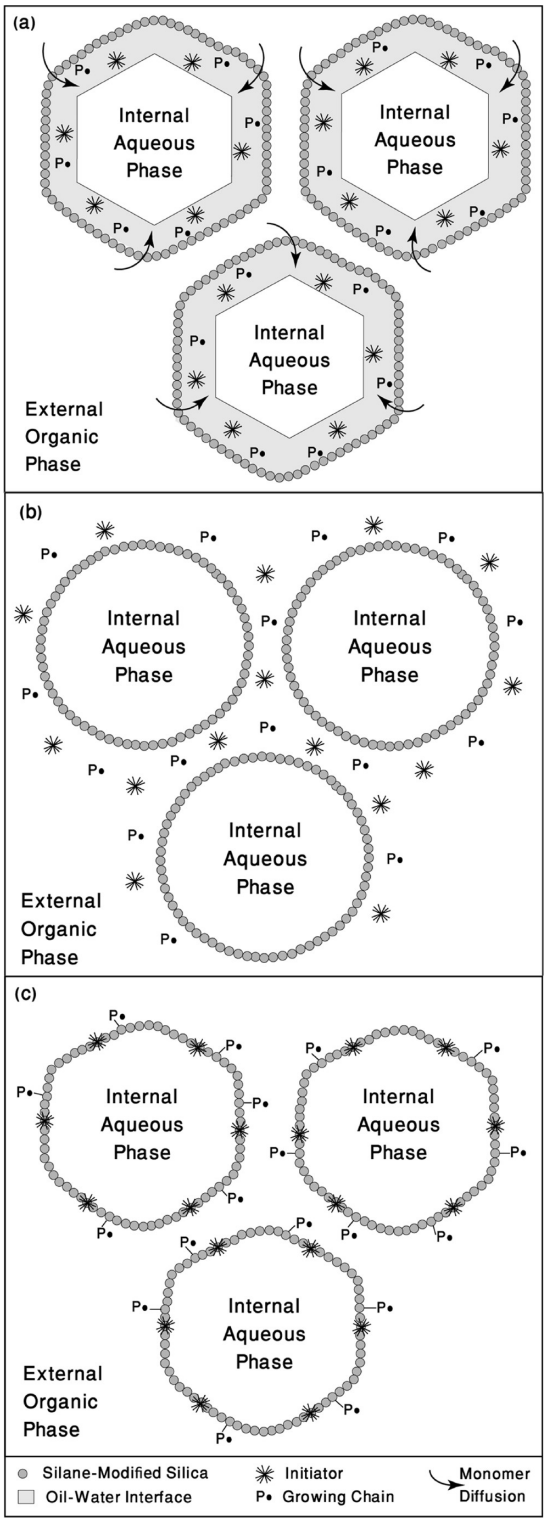

Figure 10. Schematic illustrations of polymerizations within Pickering HIPE: (a) interfacial initiation (PKM and PEM); (b) organic-phase initiation (PBM); (c) NP-based AGET ATRP initiation (PC).

demonstrate that AGET ATRP can be used as a viable alternative to conventional free radical polymerization for the synthesis of polyHIPEs with typical polyHIPE porous structures.

The contrast between the polyHIPE walls and the PMMA-filled voids is clear in Figure 6c,d for SE, which does not contain nanoparticles. The dark C-NP in SC can be easily distinguished from the polymer in the polyHIPE walls and the PMMA-filled voids in Figure 7c,d. The C-NP form aggregates which are randomly dispersed throughout the polyHIPE walls. This aggregation could reduce the effectiveness of the initiator and produce the relatively low 78.0% yield for SC compared to 96.8% for SE and similar yields for equivalent polyHIPEs from surfactant-stabilized HIPEs. The similarity of the porous structures for SE and SC indicates that the porous structure is determined by surfactant stabilization rather than by the type and locus of initiation.

The tan δ curves for SE and SC are seen in Figure 8, and the tan δ peak temperatures are listed in Table 2. These tan δ curves are typical of polyHIPEs.[11,66] All the polyHIPEs described here had similar tan δ curves. The tan δ peaks are very broad, reflecting the high degree of cross-linking that originates in the EHA:DVB mass ratios of around 4:1. The copolymerization of EHA with DVB coupled with the high degree of cross-linking yield tan δ peak temperatures that are significantly higher than the glass transition temperature of −50 °C associated with PEHA.[67]

The porous structures and wall structures of SE (Figure 6) and SC (Figure 7) are almost identical and do not seem to be affected by the type and locus of initiation. The tan δ peak temperatures of SE and SC, on the other hand, are quite different and do seem to be affected by the type and locus of initiation. The tan δ peak temperature for EBiB-initiated SE, which does not contain nanoparticles, was −20 °C. The tan δ peak temperature for the C-NP-initiated SC was 5 °C. This significant difference in tan δ peak temperatures is indicative of significant differences in the macromolecular structures.

Interfacially initiated copolymerization within a HIPE can enhance the macromolecular content of the more interfacially active monomer.[13] Here, EHA is the more interfacially active monomer. Interfacial initiation would produce macromolecules that are relatively rich in EHA and would, therefore, have a lower tan δ peak temperature. This seems to indicate that AGET ATRP using EBiB as an initiator is, in some ways, similar to interfacial initiation in conventional radical polymerization. This similarity may originate in the water-soluble catalyst system and the water-soluble reducing agent. EBiB is preferentially located in the external, organic phase while the $CuBr_2$, bpy, and AA are preferentially located in the internal, aqueous phase. The similarity between AGET ATRP using EBiB and interfacial initiation using conventional radical polymerization is supported by the analysis of polyHIPEs from Pickering HIPEs described below.

Additional factors that yield a relatively high tan δ peak temperature for SC are the initiation that occurs at the C-NP surface. A large number of macromolecules are bound to the nanoparticle surface, and therefore, the nanoparticles become cross-linking hubs. The nanoparticles are also covered with a shell of bound polymer molecules whose molecular mobility is restricted compared to macromolecules that are not bound to the nanoparticles. The 25 °C difference in the tan δ peak temperatures reflects the differences in macromolecular structure, in cross-linking, and in molecular mobility that result from the different types and loci of initiation.

Conventional Radical Initiation in Pickering HIPEs. Unlike the polyHIPEs from surfactant-stabilized HIPEs, the porous structures of polyHIPEs from the Pickering HIPEs are strongly dependent upon the type and locus of initiation. Interfacial initiation in PKM, which results from the addition of a water-soluble conventional radical initiator to the internal, aqueous phase of a HIPE, yields polyhedral voids from 60 to 115 μm (Figure 9a,b).

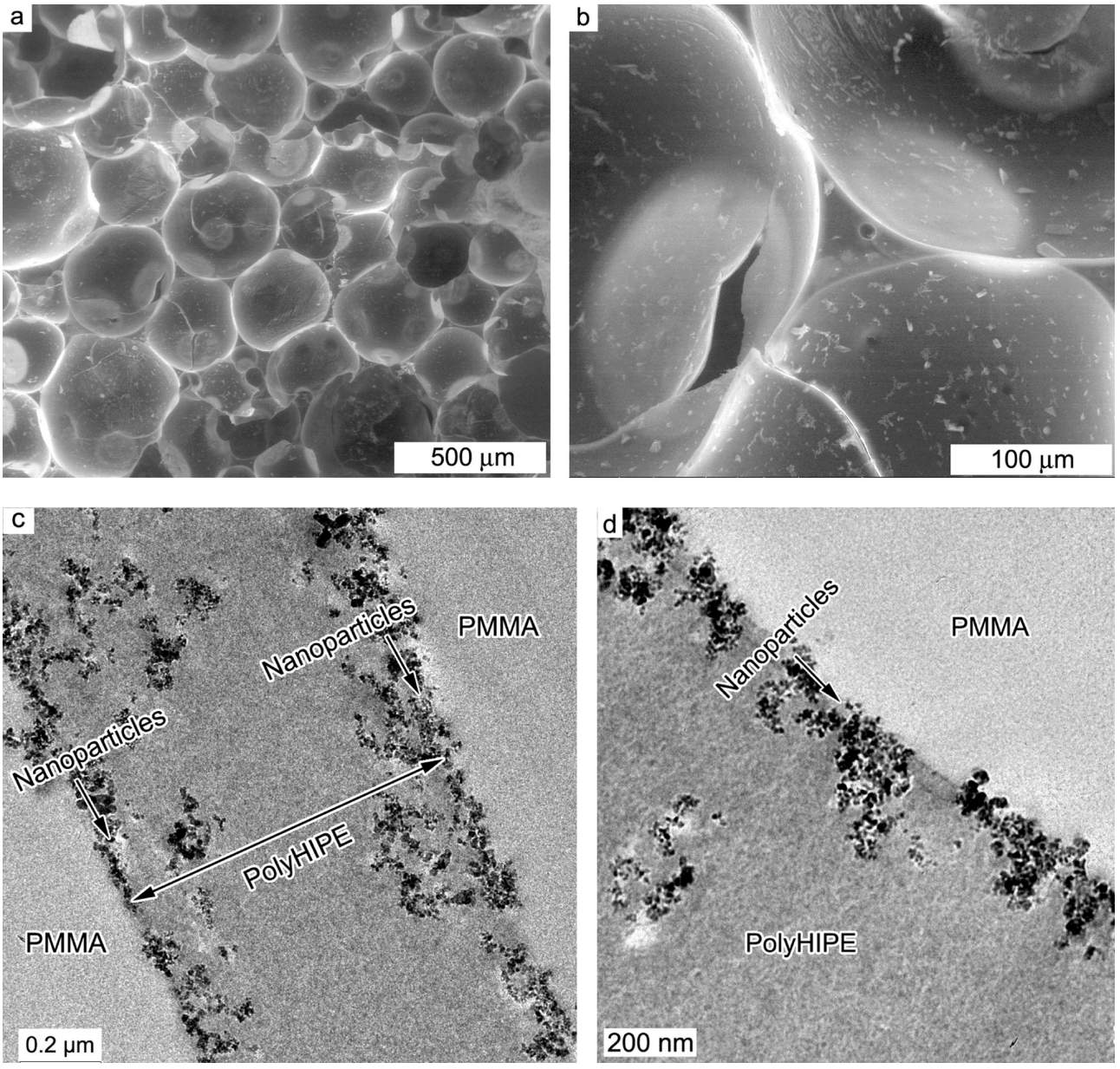

Figure 11. PBM: SEM micrographs (a, b) and TEM micrographs (c, d).

The internal phase droplets in nanoparticle-stabilized Pickering HIPEs are more than an order of magnitude greater than those in surfactant-stabilized HIPEs. The polymerization in PKM begins at the interface and "locks in" the HIPE's polyhedral droplet shape before extensive destabilization through droplet coalescence and/or Ostwald ripening can take place. Figure 9a,b does not exhibit the highly interconnected porous structure typical of polyHIPEs. However, the prevalence of the numerous cracks and flaws in the walls (Figure 9c) and the removal of the water indicate that the polyHIPE does not have a completely closed-cell structure.

The M-NP at the oil—water interface stabilizes the HIPE, and one would expect the M-NP to be located on the polyHIPE void surfaces. Figure 9d shows a cross section of the polyHIPE wall between two voids. The two parallel lines of M-NP seen in Figure 9d,e originate in the M-NP shells surrounding the internal phase droplets in the HIPE. However, the M-NP are located within the polyHIPE walls, far from the polyHIPE surface. During interfacially initiated polymerization, the monomer diffuses toward the initiation site, the oil—water interface, and polymer walls form around the M-NP shells, as illustrated schematically in Figure 10a. The M-NP move along the polymerization front, lying between the monomer-swollen polymer undergoing polymerization and the monomer reservoir in the external phase. The two polymerization fronts illustrated in Figure 10a are the darker areas lying between the void surfaces and the M-NP lines in Figure 9d,e. The monomer reservoir lies between the two polymerization fronts, the lighter area between the M-NP lines in Figure 9d,e. Unreacted monomer in the reservoir would be removed on drying the polyHIPE. Such a porous wall structure would appear lighter in the TEM.

PBM is based upon the same HIPE as PKM, except in PBM the conventional radical initiator is dissolved in the external, organic phase instead of in the internal, aqueous phase. The

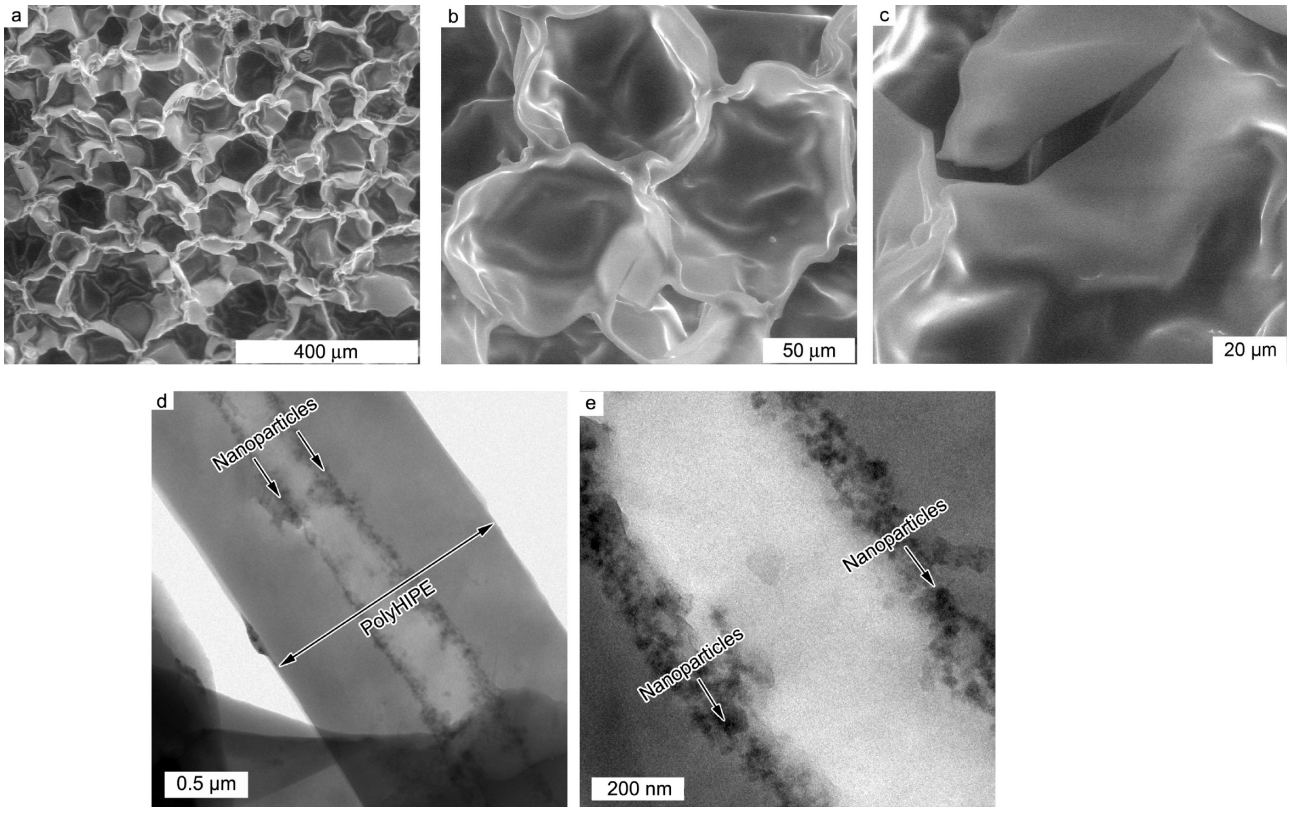

Figure 12. PEM: SEM micrographs (a−c) and TEM micrographs (d, e).

porous structure of PBM, with its spherical voids (Figure 11a,b), is completely different from that of PKM, with its polyhedral voids (Figure 9a,b). The initiation occurs simultaneously throughout the external phase. Therefore, the change to the original polyhedral HIPE droplet shape that yields the spherical droplet shape can take place through droplet coalescence and/or Ostwald ripening before the wall shape is "locked in", as illustrated schematically in Figure 10b. The change to the droplet shape is accompanied by an increase in the droplet size. The void size of around 310 μm (Figure 11a,b) is significantly larger than the void size for PKM (Figure 9a,b). PBM does not exhibit the highly interconnected porous structure typical of polyHIPEs. It does, however, have an interconnected structure resulting from the flaws and cracks that are visible in the void walls in Figure 11a,b. The M-NP are located, for the most part, at the polyHIPE surface, between the polyHIPE wall and the PMMA-filled voids, as seen in Figure 11c,d. As illustrated schematically in Figure 10b, there is no preferential diffusion of monomer toward the interface that would affect the location of the M-NP. Therefore, the M-NP remain at the oil−water interface. There are some random M-NP aggregates within the polyHIPE wall. The generation of such aggregates may result from the changes in droplet shape and size upon HIPE destabilization during polymerization.

The tan δ peak temperature for the interfacially initiated PKM is −27 °C, 16 °C lower than the tan δ peak temperature of −11 °C for organic-phase initiated PBM (Table 2). This difference between the tan δ peak temperatures is similar to that seen for the polyHIPE from surfactant-stabilized HIPEs. The tan δ peak temperature of EBiB-initiated SE was 25 °C lower than that of C-NP-initiated SC (Table 2). In that case, only SC contained nanoparticles. In this case, both PKM and PBM contain M-NP. Therefore, the difference in their tan δ peak temperatures reflects the effects of the locus of initiation on the macromolecular structure. Interfacial initiation with KPS produces relatively EHA-rich macromolecules and, therefore, a lower tan δ peak temperature. The similar tan δ peak temperatures for SE and PKM support the contention that the results from using AGET ATRP with EBiB are, in some ways, similar to those from using conventional radical polymerization with interfacial initiation.

AGET ATRP in Pickering HIPEs. While PEM is stabilized using M-NP, as were PKM and PBM, it is initiated using EBiB, as was SE. It was not clear, *a priori*, whether the results from using AGET ATRP with EBiB would be similar to those from conventional radical polymerization using interfacial initiation, similar to those from conventional radical polymerization using organic-phase initiation, or something completely different. The relatively polyhedral void shapes seen for PEM in Figure 12a,b are similar to those seen for PKM in Figure 9a,b. The voids are around 120−210 μm, twice the size in PKM. This indicates that the polymerization begins at the interface and "locks in" the polyhedral shape, as illustrated schematically in Figure 10a. Here, too, the prevalence of the numerous cracks and flaws in the walls (Figure 12c) and the removal of the water indicate that the polyHIPE does not have a completely closed-cell structure. The M-NP in PEM are located within the polyHIPE walls (Figure 12d,e), as seen previously for PKM (Figure 9d,e). Monomer diffuses toward the interface and the moving polymerization front pushes the M-NP from the oil−water interface into the wall. The two polymerization fronts are the darker areas between the voids and the M-NP lines, and the monomer reservoir is the lighter area between the M-NP lines. For the polyHIPE based on

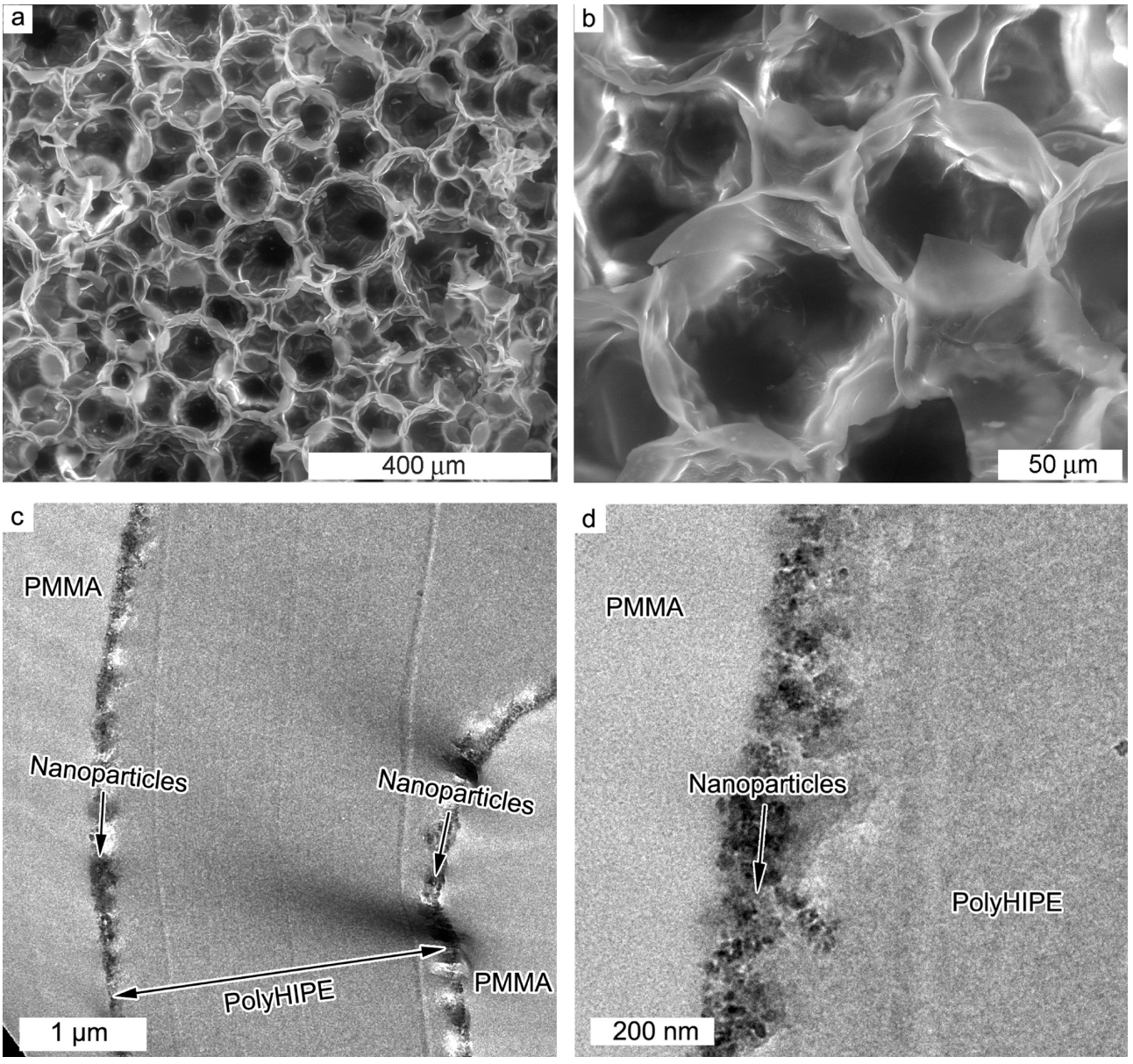

Figure 13. PC: SEM micrographs (a, b) and TEM micrographs (c, d).

Pickering HIPE, AGET ATRP with EBiB closely resembles interfacial initiation with a conventional radical initiator.

The relatively spherical voids in PC are around 75−120 μm in diameter (Figure 13a,b). These voids seem to be more spherical than those in PEM (Figure 12a,b) but less spherical than those in PBM (Figure 11a,b). In addition, the voids in PC exhibit the types of flaws and cracks seen in PBM's voids. The C-NP in PC perform two functions: they stabilize the HIPE, and they are the AGET ATRP initiator. Both of these functions can affect the void size and shape. The differences between M-NP and C-NP in surface chemistry and surface coverage could affect the size and shape of the droplets in the HIPE's internal phase. In addition, the type and locus of initiation can affect the extent of HIPE destabilization through droplet coalescence and/or Ostwald ripening.

Figure 13c,d shows a densely packed assembly of C-NP located on the polyHIPE surface (between the polyHIPE and the PMMA-filled voids). There are no C-NP aggregates randomly scattered throughout the polyHIPE wall, as seen for PBM. The C-NP stabilize the Pickering HIPE by being located at the oil−water interface. Polymerization in a Pickering HIPE using a NP-based AGET ATRP initiator located at the oil−water interface is illustrated schematically in Figure 10c. Initiation at the C-NP surface causes the nanoparticles to "lock" together at the oil−water interface from the very beginning of the polymerization.

The AGET ATRP polymerization in PEM exhibited structural similarities to the interfacially initiated PKM. This similarity is supported by PEM's tan δ peak temperature of −27 °C, which is the same as PKM's (Table 2). The similarity in tan δ peak temperatures for EBiB-initiated SE, EBiB-initiated PEM, and interfacially initiated PKM confirms the significant effect that the locus of initiation has on the macromolecular structure. The tan δ peak temperature of −11 °C for the C-NP-initiated PC may indicate that the C-NP become cross-linking hubs to which macromolecules with reduced mobility are bound. These results

demonstrate that the type and locus of initiation in polyHIPEs from Pickering HIPEs have significant effects upon the macromolecular structure, the wall structure, and the porous structure.

CONCLUSIONS

AGET ATRP has been shown to be a viable alternative to conventional radical polymerization for the synthesis of polyHIPEs from both surfactant-stabilized HIPEs and Pickering HIPEs. The porous structures of the polyHIPEs from surfactant-stabilized HIPEs were similar to those of typical polyHIPEs, whether the AGET ATRP initiator was dissolved in the organic phase or was located on the surface of nanoparticles within the organic phase. The significantly lower tan δ peak temperature that resulted when the AGET ATRP initiator was dissolved in the organic phase reflects a relatively EHA-rich macromolecular structure that can be associated with initiation that occurs at the interface. The similarity to conventional radical polymerization with interfacial initiation results from the combination of an organic-soluble AGET ATRP initiator with a water-soluble catalyst system/reducing agent.

For polyHIPEs synthesized within Pickering HIPEs, the macromolecular structure, the wall structure, and the porous structure are all dependent upon the type and locus of initiation. PolyHIPEs whose synthesis involves interfacial initiation, whether from a conventional water-soluble radical initiator or from an organic-soluble AGET ATRP initiator, exhibited lower tan δ peak temperatures that reflect relatively EHA-rich macromolecules, exhibited nanoparticles within the walls that are associated with monomer diffusion to the interface, and exhibited relatively polyhedral voids that are associated with polymerization that begins at the interface and "locks in" the structure of the original HIPE.

An organic-soluble conventional radical initiator and a nanoparticle-based AGET ATRP initiator produced polyHIPEs with higher tan δ peak temperatures, nanoparticles that are located on the void surfaces, and voids that are relatively spherical. There was no preferential diffusion of monomer to the interface for the organic-soluble conventional radical initiator, and therefore, the nanoparticles remained at the oil—water interface. The nanoparticle-based AGET ATRP initiator had two functions, it stabilized the Pickering HIPE and it initiated polymerization. When polymerization initiated at the nanoparticle surface, the polymerizing macromolecules "locked" the nanoparticles together at the HIPE's oil-water interface.

ACKNOWLEDGMENT

The partial support of the Israel Science Foundation and of the Technion VPR Fund is gratefully acknowledged.

REFERENCES

(1) Barby, D.; Haq, Z. US Patent 4,522,953, 1985.
(2) Cameron, N. R. *Polymer* **2005**, *46*, 1439–1449.
(3) Williams, J. M.; Wrobleski, D. A. *Langmuir* **1988**, *4*, 656–662.
(4) Williams, J. M.; Gray, A. J.; Wilkerson, M. H. *Langmuir* **1990**, *6*, 437–444.
(5) Cameron, N. R.; Sherrington, D. C. *Adv. Polym. Sci.* **1996**, *126*, 163–214.
(6) Cameron, N. R.; Sherrington, D. C.; Albiston, L.; Gregory, D. P. *Colloid Polym. Sci.* **1996**, *274*, 592–595.
(7) Cameron, N. R.; Krajnc, P.; Silverstein, M. S. In *Porous Polymers*; Silverstein, M. S., Cameron, N. R., Hillmyer, M. A., Eds.; John Wiley and Sons: Hoboken, NJ, 2011; Chapter 4.
(8) Silverstein, M. S.; Cameron, N. R. PolyHIPEs - Porous Polymers from High Internal Phase Emulsions. In *Encyclopedia of Polymer Science and Technology*; Wiley: New York, DOI: 10.1002/0471440264.pst571, 2010.
(9) Sergienko, A.; Tai, H.; Narkis, M.; Silverstein, M. S. *J. Appl. Polym. Sci.* **2004**, *94*, 2233–2239.
(10) Leber, N.; Fay, J. D. B.; Cameron, N. R.; Krajnc, P. *J. Polym. Sci., Part A: Polym. Chem.* **2007**, *45*, 4043–4053.
(11) Tai, H.; Sergienko, A.; Silverstein, M. S. *Polym. Eng. Sci.* **2001**, *41*, 1540–1552.
(12) Livshin, S.; Silverstein, M. S. *Macromolecules* **2007**, *40*, 6349–6354.
(13) Livshin, S.; Silverstein, M. S. *Soft Matter* **2008**, *4*, 1630–1638.
(14) Livshin, S.; Silverstein, M. S. *Macromolecules* **2008**, *41*, 3930–3938.
(15) Butler, R.; Davies, C. M.; Cooper, A. I. *Adv. Mater.* **2001**, *13*, 1459–1463.
(16) Zhang, H.; Cooper, A. I. *Chem. Mater.* **2002**, *14*, 4017–4020.
(17) Butler, R.; Hopkinson, I.; Cooper, A. I. *J. Am. Chem. Soc.* **2003**, *125*, 14473–14481.
(18) Krajnc, P.; Scarontefanec, D.; Pulko, I. *Macromol. Rapid Commun.* **2005**, *26* (16), 1289–1293.
(19) Kulygin, O.; Silverstein, M. S. *Soft Matter* **2007**, *3*, 1525–1529.
(20) Busby, W.; Cameron, N. R.; Jahoda, C. A. B. *Biomacromolecules* **2001**, *2*, 154–164.
(21) Bokhari, M. A.; Akay, G.; Zhang, S.; Birch, M. A. *Biomaterials* **2005**, *26* (25), 5198–5208.
(22) Hayman, M. W.; Smith, K. H.; Cameron, N. R.; Przyborski, S. A. *Biochem. Biophys. Methods* **2005**, *62*, 231–240.
(23) Akay, G.; Birch, M. A.; Bokhari, M. A. *Biomaterials* **2004**, *25*, 3991–4000.
(24) Stefanec, D.; Krajnc, P. *React. Funct. Polym.* **2005**, *65*, 37–45.
(25) Lumelsky, Y.; Lalush-Michael, I.; Levenberg, S.; Silverstein, M. S. *J. Polym. Sci., Part A: Polym. Chem.* **2009**, *47*, 7043–7053.
(26) Mercier, A.; Deleuze, H.; Maillard, B.; Mondain-Monval, O. *Adv. Synth. Catal.* **2002**, *344*, 33–36.
(27) Moine, L.; Deleuze, H.; Maillard, B. *Tetrahedron Lett.* **2003**, *44*, 7813–7813.
(28) Tai, H.; Sergienko, A.; Silverstein, M. S. *Polymer* **2001**, *42*, 4473–4482.
(29) Silverstein, M. S.; Tai, H.; Sergienko, A.; Lumelsky, Y.; Pavlovsky, S. *Polymer* **2005**, *46*, 6682–6694.
(30) Normatov, J.; Silverstein, M. S. *Macromolecules* **2007**, *40*, 8329–8335.
(31) Zhang, H.; Hardy, G. C.; Rosseinsky, M. J.; Cooper, A. I. *Adv. Mater.* **2003**, *15*, 78–81.
(32) Lepine, O.; Birot, M.; Deleuze, H. *J. Polym. Sci., Part A: Polym. Chem.* **2007**, *45* (18), 4193–4203.
(33) Normatov, J.; Silverstein, M. S. *Chem. Mater.* **2008**, *20*, 1571–1577.
(34) Menner, A.; Powell, R.; Bismarck, A. *Soft Matter* **2006**, *4*, 337–342.
(35) Haibach, K.; Menner, A.; Powell, R.; Bismarck, A. *Polymer* **2006**, *47*, 4513–4519.
(36) Menner, A.; Haibach, K.; Powell, R.; Bismarck, A. *Polymer* **2006**, *47*, 7628–7635.
(37) Desforges, A.; Backov, R.; Deleuze, H.; Mondain-Monval, O. *Adv. Funct. Mater.* **2005**, *15*, 1689–1695.
(38) Richez, A.; Deleuze, H.; Vedrenne, P.; Collier, R. *J. Appl. Polym. Sci.* **2005**, *96* (6), 2053–2063.
(39) David, D.; Silverstein, M. S. *J. Polym. Sci, Part A: Polym. Chem.* **2009**, *47*, 5806–5814.
(40) Deleuze, H.; Faivre, R.; Herroguez, V. *Chem. Commun.* **2002**, 2822–2823.
(41) Gitli, T.; Silverstein, M. S. *Soft Matter* **2008**, *4*, 2475–2485.
(42) Gitli, T.; Silverstein, M. S. *Polymer* **2011**, *52*, 107–115.
(43) Gurevitch, I.; Silverstein, M. S. *J. Polym. Sci., Part A: Polym. Chem.* **2010**, *48*, 1516–1525.

(44) Pickering, S. U. *J. Chem. Soc.* **1907**, *91*, 2001–2021.
(45) Binks, B. P.; Lumsdon, S. O. *Langmuir* **2000**, *16*, 8622–8631.
(46) Binks, B. P.; Fletcher, P. D. I. *Langmuir* **2001**, *17*, 4708–4710.
(47) Colver, P. J.; Bon, S. A. F. *Chem. Mater.* **2007**, *19*, 1537–1539.
(48) Menner, A.; Ikem, V.; Salgueiro, M.; Shaffer, M. S. P.; Bismarck, A. *Chem. Commun.* **2007**, 4274–4276.
(49) Menner, A.; Verdejo, R.; Shaffer, M.; Bismarck, A. *Langmuir* **2007**, *23*, 2398–2403.
(50) Ikem, V. O.; Menner, A.; Bismarck, A. *Angew. Chem., Int. Ed.* **2008**, *47*, 8277–8279.
(51) Zhang, S.; Chen, J. *Chem. Commun.* **2009**, 2217–2219.
(52) Cummins, D.; Wyman, P.; Duxbury, C. J.; Thies, J.; Koning, C. E.; Heise, A. *Chem. Mater.* **2007**, *19*, 5285–5292.
(53) Min, K.; Gao, H.; Matyjaszewski, K. *J. Am. Chem. Soc.* **2005**, *127*, 3825–3830.
(54) Min, K.; Jakubowski, W.; Matyjaszewski, K. *Macromol. Rapid Commun.* **2006**, *27*, 594–598.
(55) Min, K.; Gao, H.; Matyjaszewski, K. *J. Am. Chem. Soc.* **2006**, *128*, 10521–10526.
(56) Oh, J. K.; Tang, C.; Gao, H.; Tsarevsky, N. V.; Matyjaszewski, K. *J. Am. Chem. Soc.* **2006**, *128*, 5578–5584.
(57) Matyjaszewski, K.; Dong, H.; Jakubowski, W.; Pietrasik, J.; Kusumo, A. *Langmuir* **2007**, *23*, 4528–4531.
(58) Min, K.; Gao, H.; Yoon, J. A.; Wu, W.; Kowalewski, T.; Matyjaszewski, K. *Macromolecules* **2009**, *42*, 1597–1603.
(59) Min, K.; Matyjaszewski, K. *Cent. Eur. J. Chem.* **2009**, *7*, 657–674.
(60) Fu, G. D.; Zhao, J. P.; Sun, Y. M.; Kang, E. T.; Neoh, K. G. *Macromolecules* **2007**, *40*, 2271–2275.
(61) Ohno, K.; Morinaga, T.; Koh, K.; Tsujii, Y.; Fukuda, T. *Macromolecules* **2005**, *38*, 2137–2142.
(62) Pyun, J.; Matyjaszewski, K.; Kowalewski, T.; Savin, D.; Patterson, G.; Kickelbick, G.; Huesing, N. *J. Am. Chem. Soc.* **2001**, *123*, 9445–9446.
(63) Saleh, N.; Sarbu, T.; Sirk, K.; Lowry, G. V.; Matyjaszewski, K.; Tilton, R. D. *Langmuir* **2005**, *21*, 9873–9878.
(64) Liu, B.; Wei, W.; Qu, X.; Yang, Z. *Angew. Chem., Int. Ed.* **2008**, *47*, 3973–3975.
(65) Carnachan, R. J.; Bokhari, M.; Przyborski, S. A.; Cameron, N. R. *Soft Matter* **2006**, *2*, 608–616.
(66) Sergienko, A. Y.; Tai, H. W.; Narkis, M.; Silverstein, M. S. *J. Appl. Polym. Sci.* **2002**, *84*, 2018–2027.
(67) Andrews, R. A.; Grulke, E. A. In *Polymer Handbook*, 4th ed.; Brandrup, J., Immergut, E. H., Grulke, E. A., Eds.; John Wiley and Sons: NewYork, 1999; p VI/200.